Role of the Meso Substituent in Defining the Reduction of Uranyl Dipyrrin Complexes

Citation for published version:
Van Rees, K, Rajeshkumar, T, Maron, L, Sproules, S & Love, JB 2022, 'Role of the Meso Substituent in Defining the Reduction of Uranyl Dipyrrin Complexes', *Inorganic Chemistry*.
https://doi.org/10.1021/acs.inorgchem.2c03048

Digital Object Identifier (DOI):
10.1021/acs.inorgchem.2c03048

Published In:
Inorganic Chemistry

Inorganic Chemistry

pubs.acs.org/IC Article

Role of the Meso Substituent in Defining the Reduction of Uranyl Dipyrrin Complexes

Karlotta van Rees, Thayalan Rajeshkumar, Laurent Maron, Stephen Sproules, and Jason B. Love*

Cite This: *Inorg. Chem.* 2022, 61, 20424−20432 Read Online

ACCESS | Metrics & More | Article Recommendations | Supporting Information

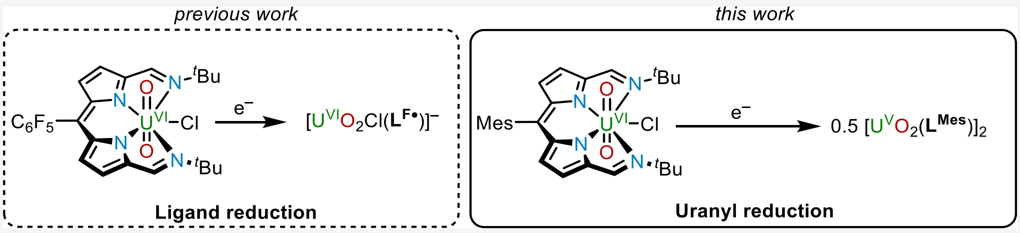

ABSTRACT: The uranyl complex $U^{VI}O_2Cl(\mathbf{L}^{Mes})$ of the redox-active, acyclic dipyrrin−diimine anion $\mathbf{L}^{Mes-}$ [$H\mathbf{L}^{Mes}$ = 1,9-di-*tert*-butyl-imine-5-(mesityl)dipyrrin] is reported, and its redox property is explored and compared with that of the previously reported $U^{VI}O_2Cl(\mathbf{L}^{F})$ [$H\mathbf{L}^{F}$ = 1,9-di-*tert*-butyl-imine-5-(pentafluorophenyl)dipyrrin] to understand the influence of the meso substituent. Cyclic voltammetry, electron paramagnetic resonance spectroscopy, and density functional theory studies show that the alteration from an electron-withdrawing meso substituent to an electron-donating meso substituent on the dipyrrin ligand significantly modifies the stability of the products formed after reduction. For $U^{VI}O_2Cl(\mathbf{L}^{Mes})$, the formation of a diamond-shaped, oxo-bridged uranyl(V) dimer, $[U^{V}O_2(\mathbf{L}^{Mes})]_2$ is seen, whereas in contrast, for $U^{VI}O_2Cl(\mathbf{L}^{F})$, only ligand reduction occurs. Computational modeling of these reactions shows that while ligand reduction followed by chloride dissociation occurs in both cases, ligand-to-metal electron transfer is favorable for $U^{VI}O_2Cl(\mathbf{L}^{Mes})$ only, which subsequently facilitates uranyl(V) dimerization.

INTRODUCTION

The single-electron reduction of the ubiquitous and inert uranyl(VI) dication, UO_2^{2+}, is an important facet in environmental uranium remediation due to the easy disproportionation of the uranyl(V) cation, UO_2^{+}, into immobile uranium(IV).[1] Significant advances have been made in the study of the direct reduction chemistry of uranyl(VI) using anaerobic techniques, resulting in a wide variety of isolable, often oxo-functionalized uranyl(V) complexes, some of which show significant stability in air.[2]

An alternative route to reduced uranium chemistry is to pair the uranyl(VI) cation with a redox-active ligand. Studies of uranyl(VI) complexes of redox-active ligands have been reported for Schiff bases,[3−5] quinones,[6] pyrroles, tetraaza[14]-annulenes,[7] NacNac,[8] calix[4]pyrroles,[9] and dipyrrins.[10−12] Recently, it was shown that uranyl(VI) complexes of pentadentate N_3O_2−saldien ligands underwent metal-based, one-electron reduction only, with a clear increase in the $U^{VI/V}$ reduction potential associated with an increase in the electron-withdrawing nature of the substituents.[13] In contrast, uranyl(VI) complexes of α-di-iminediphenolate or salophen ligands undergo single-electron ligand reductions, leading to the uranyl(VI) ligand-centered radical anions and not the expected uranyl(V) complexes.[3,4,14] Lastly, uniquely redox-active and water stable uranyl(V) complexes of dipicolinate and amino-carboxylate ligands have been reported.[15]

We recently reported the redox behavior of uranyl(VI) complexes of the donor-expanded Schiff-base dipyrrin (**1**) (Scheme 1).[11,12] The reaction of **1** with the outer-sphere reductant $CoCp_2$ resulted in a single-electron reduction of the ligand to form the uranyl(VI) dipyrrin radical complex, $[Cp_2Co][U^{VI}O_2Cl(\mathbf{L}^{F\bullet})]$ (**2**); the addition of a second equivalent of $CoCp_2$ reduced the uranium center to uranyl(V). In this case, the lowest unoccupied molecular orbital (LUMO) of **1** was found to be ligand-based, and while this favored

Scheme 1. Previous Work Carried out on $U^{VI}O_2Cl(L^F)$, (1)[a]

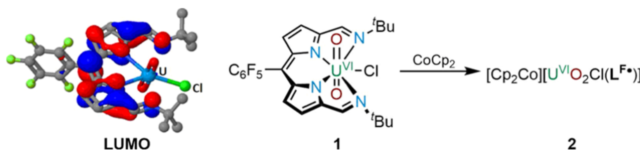

[a]The molecular orbital plot of **1**. The ISO value is 0.02 au. Positive is blue; negative is red.

Received: August 26, 2022
Published: December 6, 2022

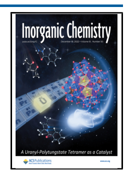

https://doi.org/10.1021/acs.inorgchem.2c03048
Inorg. Chem. 2022, 61, 20424−20432

outer-sphere ligand reduction, the metal reduction could be promoted using the inner-sphere reductant $[Cp_2TiCl]_2$ through Lewis acid activation of the uranyl oxo group, which diminished the $U^{VI/V}$ reduction potential.

It is known that modifying the *meso*-carbon substituent of the dipyrrin ligand can influence geometry and chemistry due to steric and electronic effects.[16] It was therefore envisaged that modifying the *meso*-carbon substituent in **1** from the electron-withdrawing C_6F_5 group to the electron-donating mesityl ($C_6H_2Me_3$-2,4,6) may flip the redox chemistry of its uranyl complex, from ligand-based to metal-based. This study presents the formation of new uranyl(VI) complexes of a dipyrrin−diimine ligand and an evaluation of its reduction properties. The incorporation of the electron-donating mesityl meso substituent is found to change significantly the stability of the products formed after one-electron reduction.

■ EXPERIMENTAL SECTION

General Procedure. **Caution**: Depleted uranium (primary isotope ^{238}U) is a weak α-emitter (4.197 MeV) with a half-life of 4.47×10^9 years. Manipulations and reactions should be carried out in monitored fume hoods or in an inert atmosphere glovebox in a radiation laboratory equipped with α- and β-counting equipment.

The syntheses of all air- and moisture-sensitive compounds were carried out using standard Schlenk techniques under an atmosphere of dry argon. Vacuum atmospheres and MBraun gloveboxes were used to manipulate and store air- and moisture-sensitive compounds under an atmosphere of dried and deoxygenated dinitrogen. The solvents benzene-d_6 and pyridine-d_5 were refluxed over potassium metal overnight, trap-to-trap distilled, and free-pump−thaw degassed three times prior to use. All glassware was dried in an oven at 160 °C, cooled under 10^{-3} mbar vacuum, and then purged with argon. Prior to use, all Fisherbrand *R* 1.2 mm retention glass microfiber filters and stainless-steel cannulae were dried in an oven at 160 °C overnight. All solvents for use with air- and moisture-sensitive compounds were stored in Teflon-tapped ampoules containing pre-dried 4 Å molecular sieves. Dry solvents were collected from a solvent purification system (Innovation Technologies). All chemicals were used as received without any purification, unless otherwise specified. Tetrabutylammonium hexafluorophosphate, $[^nBu_4N][PF_6]$, was recrystallized twice from absolute ethanol and dried for 2 days under vacuum.

^{1}H NMR spectra were recorded on a Bruker AVA400 spectrometer operating at 399.90 MHz, a Bruker AVA500 or a Bruker PRO500 operating at 500.12 MHz, or a Bruker AVA600 spectrometer operating at 599.81 MHz. ^{13}C{^{1}H} NMR spectra were recorded on a Bruker AVA500 or a Bruker PRO500 operating at 125.76 MHz. ^{19}F{^{1}H} NMR spectra were recorded on a Bruker AVA500 spectrometer operating at 470.59 MHz. Chemical shifts are reported in parts per million (ppm). ^{1}H and ^{13}C{^{1}H} NMR spectra are referenced to residual solvent resonances calibrated against the external standard, $SiMe_4$ (δ = 0 ppm). ^{19}F{^{1}H} NMR spectra are referenced to the external standard, CCl_3F (δ = 0 ppm). All spectra were recorded at 298 K unless otherwise specified. All data were processed using MestReNova 12.0.3. Full assignment of the NMR data is provided in the Supporting Information.

Single-crystal X-ray diffraction data were collected at 120 K on an Oxford Diffraction Excalibur diffractometer using graphite monochromated Mo K_α radiation equipped with an Eos charge-coupled device detector (λ = 0.71073 Å), or at 120 K on a Supernova, Dual, Cu at zero Atlas diffractometer using Cu K_α radiation (λ = 1.5418 Å). Structures were solved using ShelXT direct methods or intrinsic phasing and refined using a full-matrix least-squares refinement on $|F|^2$ using ShelXL.[17] All programs were used within the Olex suite.[18] All non-hydrogen atoms were refined with anisotropic displacement parameters, and hydrogen atom parameters were constrained to parent atoms and refined using a riding model unless otherwise specified. All X-ray crystal structures were analyzed and illustrated using Mercury 4.3.1.

Elemental analyses were recorded in duplicate by Mr. Stephen Boyer at the London Metropolitan University and by Elemental Microanalysis Ltd. All Fourier transform infrared (FTIR) spectra were recorded using JASCO 410 or JASCO 460 plus spectrometers. Intensities are assigned as w = weak, m = medium, and s = strong. All UV−vis absorption spectra were recorded on a Jasco V-670 spectrometer on a 10 mm quartz cuvette, fitted with a septum for air-sensitive compounds.

Synthesis. ***HL^Mes^***. 1,9-Diformyl-5-(mesityl)dipyrromethane[19] (2.2 g, 6.9 mmol, 1 equiv) was dissolved in $PhCH_3$ (300 mL). After the addition of Na_2SO_4 (4.4 g, 30.9 mmol, 4.5 equiv) and *tert*-butylamine (4.9 mL, 46.7 mmol, 6.8 equiv), the reaction mixture was heated at 50 °C for 48 h. The mixture was filtered, and the solvent was removed under reduced pressure, leaving behind a dark red oil, which was redissolved *n*-hexane (25 mL). The formed black solid was removed *via* filtration, and the remaining solvent was removed under reduced pressure, yielding HL^{Mes} as a dark red solid. Yield = 2.4 g (82%). Reddish-brown block-shaped crystals of HL^{Mes} suitable for single-crystal X-ray diffraction were grown at −20 °C from a concentrated CH_2Cl_2 solution. ^{1}H NMR (500 MHz, chloroform-*d*): δ_H 12.63 (br s, 1H, N$\underline{H}$), 8.30 (s, 2H, imine), 6.92 (s, 2H, *m*-Mes-C$\underline{H}$), 6.71 (d, *J* = 4.3 Hz, 2H, β-pyrrole), 6.38 (d, *J* = 4.2 Hz, 2H, β-pyrrole), 2.35 (s, 3H, *p*-Mes-CC$\underline{H}_3$), 2.08 (s, 6H, *o*-Mes-CC$\underline{H}_3$), 1.32 (s, 18H, ^{t}Bu-C(C$\underline{H}_3$)$_3$). ^{13}C{^{1}H} NMR (126 MHz, chloroform-*d*): δ_C 153.65 (α-pyrrole), 149.38 (imine), 142.57 (α-pyrrole), 140.43 (*o*-Mes-$\underline{C}$CH$_3$), 137.66 (*p*-Mes-$\underline{C}$CH$_3$), 136.70 (*ipso*-Mes), 133.10 (*meso*-$\underline{C}$), 128.10 (*m*-Mes-$\underline{C}$H), 127.87 (β-pyrrole), 118.74 (β-pyrrole), 57.82 (^{t}Bu-$\underline{C}$(CH$_3$)$_3$), 29.67 (^{t}Bu-C($\underline{C}$H$_3$)$_3$), 21.12 (*p*-Mes-C$\underline{C}$H$_3$), 19.93 (*o*-Mes-C$\underline{C}$H$_3$). FTIR (film) ν_{max}: 1576 cm^{-1}. UV−vis (THF): λ_{max} 272.5 nm, ε = 55 206 M^{-1} cm^{-1}; λ 476 nm, ε = 36 961 M^{-1} cm^{-1}. Elemental analysis: $C_{28}H_{36}N_4$ (MW = 428.3 g mol^{-1}) requires C, 78.46; H, 8.47; N, 13.07%. Found: C, 78.22; H, 8.61; N, 12.91%. MS (MALDI-TOF, ACN) *m/z*: [MH]$^+$ requires 429.301, found 429.301. HRMS (ESI$^+$, EtOH) *m/z*: $C_{28}H_{37}N_4$ [M + H]$^+$ requires 429.30127, found 429.30120 (mass error = −0.07 ppm).

K(L^Mes^). The synthesis was conducted under an inert atmosphere. In an ampoule, KH (16 mg, 0.4 mmol, 1.5 equiv) was suspended in anhydrous tetrahydrofuran (THF) (10 mL) and cooled to 0 °C. A solution of HL^{Mes} in THF (110 mg, 0.3 mmol, 1 equiv; 10 mL) was added dropwise, and the mixture was allowed to slowly warm to room temperature (RT), causing the reaction mixture to slowly change color from dark orange brown to pinkish purple. The solution was stirred for 16 h at RT before being filtered. The solvent was evaporated under reduced pressure, leaving a golden purple solid that was subsequently dried overnight under reduced pressure at 55 °C. Yield = 100 mg (86%). Greenish-pink needle-shaped crystals suitable for single-crystal X-ray diffraction were obtained at −20 °C from an *n*-hexane/THF solution (1:1). ^{1}H NMR (500 MHz, benzene-d_6): δ_H 8.18 (m, 2H, imine), 6.99 (s, 2H, *m*-Mes-C$\underline{H}$), 6.92 (m, 2H, β-pyrrole), 6.76 (m, 2H, β-pyrrole), 2.46 (s, 6H, *o*-Mes-CC$\underline{H}_3$), 2.29 (s, 3H, *p*-Mes-CC$\underline{H}_3$), 0.99 (s, 18H, ^{t}Bu-C(C$\underline{H}_3$)$_3$). ^{13}C{^{1}H} NMR (126 MHz, benzene-d_6): δ_C 156.24 (α-pyrrole), 154.01 (imine), 152.64 (α-pyrrole), 145.97 (*o*-Mes-$\underline{C}$CH$_3$), 139.20 (*p*-Mes-$\underline{C}$CH$_3$), 136.55 (*ipso*-Mes), 136.04 (*meso*-$\underline{C}$), 130.64 (β-pyrrole), 127.98 (*m*-Mes-$\underline{C}$H), 120.91 (β-pyrrole), 55.91 (^{t}Bu-$\underline{C}$(CH$_3$)$_3$), 29.70 (^{t}Bu-C($\underline{C}$H$_3$)$_3$), 20.92 (*p*-Mes-C$\underline{C}$H$_3$), 20.07 (*o*-Mes-C$\underline{C}$H$_3$). UV−vis (THF): λ_{max} 568 nm, ε = 46 315 M^{-1} cm^{-1}; λ 483 nm, ε = 15 146 M^{-1} cm^{-1}; λ 297 nm, ε = 22 163 M^{-1} cm^{-1}; λ 275 nm, ε = 24 385 M^{-1} cm^{-1}; λ 222 nm, ε = 18 654 M^{-1} cm^{-1}. Elemental analysis: $C_{28}H_{35}KN_4$ (MW = 466.3 g mol^{-1}) requires C, 72.06; H, 7.56; N, 12.00%. Found: C, 66.34; H, 7.27; N, 10.45% (unsatisfactory due to the rapid hydrolysis of the complex). HRMS (APPI$^+$, THF) *m/z*: $C_{28}H_{36}KN_4$ [M + H]$^+$ requires 467.25716, found 467.257770 (mass error = 1.30 ppm).

$U^{VI}O_2Cl(L^{Mes})$. **Method A**: K(L^{Mes}) was prepared *in situ* by the synthesis process described above using KH (71 mg, 1.8 mmol, 1.5 equiv) and HL^{Mes} in anhydrous THF (490 mg, 1.2 mmol, 1 equiv; 10 mL). The solution was stirred for 16 h before being filtered into a Schlenk tube containing a solution of $U^{VI}O_2Cl_2(THF)_2$ in THF (560 mg, 1.2 mmol, 1 equiv; 5 mL) and stirred for an additional 16 h, during which the mixture turned deep purple. The mixture was filtered, and the solvent was evaporated under reduced pressure, leaving $U^{VI}O_2Cl(\mathbf{L^{Mes}})$ as a deep purple sold. Yield = 810 mg (94%). Golden-pink block-shaped crystals suitable for single-crystal X-ray diffraction were grown at −20 °C from an *n*-hexane/THF solution (1:1). ^{1}H NMR (500 MHz, benzene-d_6): δ_H 8.80 (s, 2H, imine), 6.90 (d, *J* = 4.2 Hz, 2H, *β*-pyrrole), 6.86−6.81 (m, 2H, *m*-Mes-C$\underline{H}$), 6.59 (d, *J* = 4.2 Hz, 2H, *β*-pyrrole), 2.24 (s, 3H, *p*-Mes-CC$\underline{H}_3$), 2.15 (s, 6H, *o*-Mes-CC$\underline{H}_3$), 1.92 (s, 18H, ^{t}Bu-C(C$\underline{H}_3$)$_3$). ^{13}C{^{1}H} NMR (126 MHz, benzene-d_6): δ_C 157.79 (*α*-pyrrole), 157.54 (imine), 153.86 (*meso*-$\underline{C}$), 147.26 (*α*-pyrrole), 137.82 (*p*-Mes-$\underline{C}$CH$_3$), 136.57 (*ipso*-Mes), 135.06 (*o*-Mes-$\underline{C}$CH$_3$), 133.75 (*β*-pyrrole), 127.98 (*m*-Mes-$\underline{C}$H), 122.79 (*β*-pyrrole), 64.87 (tBu-$\underline{C}$(CH$_3$)$_3$), 30.37 (^{t}Bu-C-($\underline{C}$H$_3$)$_3$), 20.81 (*p*-Mes-C$\underline{C}$H$_3$), 19.70 (*o*-Mes-C$\underline{C}$H$_3$). UV−vis (THF): λ_{max} 584.5 nm, ε = 9210 M^{-1} cm^{-1}; λ 539 nm, ε = 5526 M^{-1} cm^{-1}; λ 292 nm, ε = 15 421 M^{-1} cm^{-1}. Elemental analysis: $C_{28}H_{35}ClN_4O_2U$ (MW = 732.3 g mol^{-1}) requires C, 45.88; H, 4.81; N, 7.64%. Found: C, 45.55; H, 4.91; N, 6.94%. HRMS (APPI$^+$, THF) *m*/*z*: $C_{28}H_{36}UO_2N_4Cl$ [M + H]$^+$ requires 733.30291, found 733.307575 (mass error = 6.36 ppm); $C_{28}H_{35}UO_2N_4$ [M − Cl]$^+$ requires 697.32624, found 697.326611 (mass error = 0.53 ppm).

[U^{V}O$_2$(L^{Mes})]$_2$. The synthesis was conducted under an inert atmosphere. A deep purple solution of $U^{VI}O_2Cl(\mathbf{L^{Mes}})$ in C_6D_6 (100 mg, 0.1 mmol, 1 equiv; 2 mL) was added to a solution of $CoCp_2$ in benzene (25 mg, 0.1 mmol, 1 equiv; 2 mL). The solution was stirred for 1 h at RT, during which a golden purple precipitate formed, which was isolated by centrifuging. Yield = 68 mg (76%). Golden-pink plate-shaped crystals suitable for single-crystal X-ray diffraction of $[U^VO_2(\mathbf{L^{Mes}})]_2$ were grown by slowly cooling a heated concentrated benzene-d_6 solution in a Teflon-tapped NMR tube. ^{1}H NMR (500 MHz, pyridine-d_5): δ_H 3.14 (s, 1H, *m*-Mes-C$\underline{H}$), 1.63 (s, 1H, *m*-Mes-C$\underline{H}$), −0.33 (br s, 3H, *p*-Mes-CC$\underline{H}_3$), −0.59 (s, 3H, *o*-Mes-CC$\underline{H}_3$), −1.90 (s, 3H, *o*-Mes-CC$\underline{H}_3$), −4.94 (br s, 2H, *β*-pyrrole), −5.41 (br s, 2H, *β*-pyrrole), −6.12 (br s, 12H, ^{t}Bu-C(C$\underline{H}_3$)$_3$), −6.22 (br s, 6H, ^{t}Bu-C(C$\underline{H}_3$)$_3$), −9.17 (s, 2H, imine). ^{13}C{^{1}H} NMR (126 MHz, pyridine-d_5): δ_C 132.19, 126.82, 122.15, 121.28, 118.63, 116.91, 101.73, 77.22, 76.00, 67.60, 32.52, 29.39, 25.58, 20.11, 17.50, 16.04, 14.48. HRMS (APPI$^+$, THF) *m*/*z*: $C_{56}H_{70}N_8O_4U_2$ [M]$^+$ requires 1394.653033, found 1394.668864 (mass error = 11.35 ppm); $C_{28}H_{35}UO_2N_4$ [0.5M]$^+$ requires 697.32624, found 697.327537 (mass error = 1.85 ppm). Elemental analysis: $C_{56}H_{70}N_8O_4U_2$ (MW = 1395.29 g mol^{-1}) requires C, 48.21; H, 5.06; N, 8.03%. Found: C, 48.55; H, 5.27; N, 8.19%.

■ RESULTS

Synthesis and Structure of Uranyl(VI) Complexes. The dipyrrin ligand $\mathrm{H}\mathbf{L^{Mes}}$ is obtained in 82% yield through a straightforward aerobic condensation/oxidation reaction between the mono-meso-substituted dipyrromethane dialdehyde

Scheme 2. Synthesis of Ligand HL^{Mes}

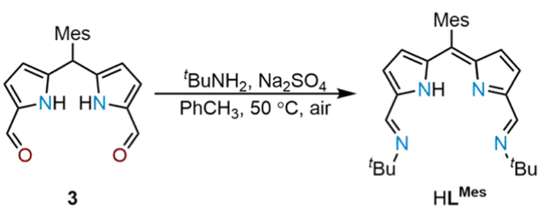

3 and excess *tert*-butylamine in toluene at RT (Scheme 2). The ^{1}H NMR spectrum of $\mathrm{H}\mathbf{L^{Mes}}$ depicts an imine proton resonance at 8.30 ppm and two resonances at 2.35 and 2.08 ppm for the mesityl group, indicating a C_{2v} symmetry in solution. Two doublets at 6.72 and 6.39 ppm are assigned to the *β*-pyrrole protons, and the singlet at 1.32 ppm is assigned to the *tert*-butyl group. In addition, the disappearance of the *meso*-proton resonance reveals that spontaneous oxidation of the dipyrromethane to the dipyrrin has occurred, similar to that seen previously in the synthesis of other Schiff base dipyrrins.[20]

Reddish-brown block-shaped single crystals of $\mathrm{H}\mathbf{L^{Mes}}$ suitable for X-ray diffraction were grown from a concentrated diethyl ether solution at −30 °C (Figure 1). While the data are poor, the connectivity is clear with the planar sp^2 hybridized *meso*-carbon further confirming the spontaneous oxidation of the ligand during its synthesis.

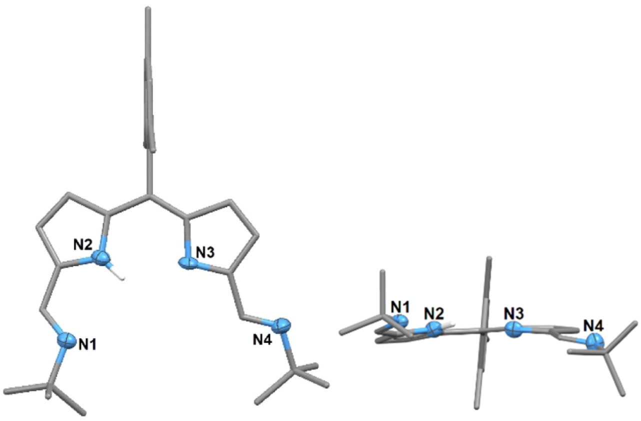

Figure 1. Solid-state structure of HL^{Mes}. For clarity, all hydrogen atoms except that of NH are omitted (where shown, displacement ellipsoids are drawn at 50% probability). Carbon atoms are gray.

The reaction between $\mathrm{H}\mathbf{L^{Mes}}$ and 1 equiv of KH in anhydrous THF cleanly generates the potassium complex K($\mathbf{L^{Mes}}$), which is isolated as a golden purple solid in 86% yield. The ^{1}H NMR spectrum of K($\mathbf{L^{Mes}}$) shows the disappearance of the NH proton, while the imine proton resonance is at 8.18 ppm and the *β*-pyrrole protons appear at 6.92 and 6.76 ppm. The mesityl methyl protons appear at 2.46 and 2.29 ppm, indicative of top/bottom symmetry.

Greenish-purple needle-shaped crystals of K($\mathbf{L^{Mes}}$) suitable for X-ray diffraction were grown from a concentrated 1:1 THF/*n*-hexane solution at −30 °C (Figure 2). The crystal is

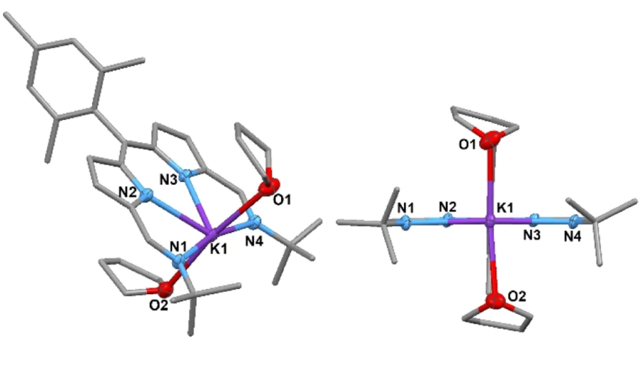

Figure 2. Solid-state structure of K($\mathbf{L^{Mes}}$)·(THF)$_2$ viewed from the top (left) and side (right). For clarity, all hydrogen atoms and one molecule are omitted (displacement ellipsoids are drawn at 50% probability). Selected bonds (Å) and angles (deg): K1−N1, 2.897(3); K1−N2, 2.732(4); K1−N3, 2.715(3); K1−N4, 2.916(3); K1−O1, 2.761(3); K1−O2, 2.799(3); N1−K1−N2, 61.65(9); N2−K1−N3, 66.40(9); N3−K1−N4, 62.28(9); N4−K1−N1, 169.56(9); O1−K1−O2, 171.36(9); C20−C10−C9, 128.2(4); C9−C10−C11, 116.5(4); and C11−C10−C20, 115.3(4).

https://doi.org/10.1021/acs.inorgchem.2c03048
Inorg. Chem. 2022, 61, 20424−20432

the THF solvate of K($\mathbf{L}^{\mathbf{Mes}}$) and exhibits a distorted octahedral geometry with the ligand coordinating in the equatorial plane in an N_4 coordination mode. There is no steric hindrance between the ligand and the coordinated potassium metal, indicated by the insignificant distance of 0.035 Å between the plane of the N_4 donor set and the potassium atom.

The uranyl complex $U^{VI}O_2Cl(\mathbf{L}^{\mathbf{Mes}})$ was prepared by two different methods. Method A is a transmetalation reaction between 1 equiv of K($\mathbf{L}^{\mathbf{Mes}}$) with an equimolar amount of $U^{VI}O_2Cl_2(THF)_2$ (Scheme 3), whereas method B reacts $H\mathbf{L}^{\mathbf{Mes}}$ with a 1:1 mixture of $U^{VI}O_2\{N(SiMe_3)_2\}_2(THF)_2$ and $U^{VI}O_2Cl_2(THF)_2$ in benzene (see the Supporting Information). The ^1H NMR spectrum of $U^{VI}O_2Cl(\mathbf{L}^{\mathbf{Mes}})$ has an imine resonance at 8.80 and the β-pyrrole protons at 6.90 and 6.59 ppm. Two singlets corresponding to the mesityl methyl groups at 2.24 and 2.15 ppm are indicative of C_{2v} symmetry.

Scheme 3. Synthesis of $U^{VI}O_2Cl(\mathbf{L}^{\mathbf{Mes}})$ by Transmetalation with K($\mathbf{L}^{\mathbf{Mes}}$) (Method A) and Directly from $H\mathbf{L}^{\mathbf{Mes}}$ (Method B)

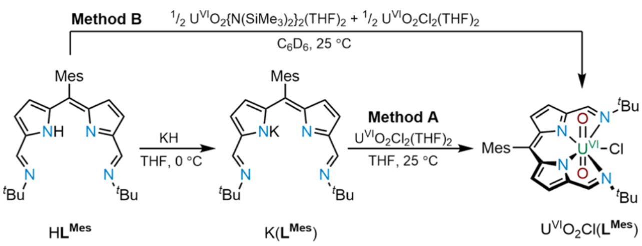

Purplish-golden block-shaped single crystals of $U^{VI}O_2Cl$-($\mathbf{L}^{\mathbf{Mes}}$) were grown from a concentrated 1:1 THF/n-hexane solution at −30 °C (Figure 3). In the solid state, the uranium

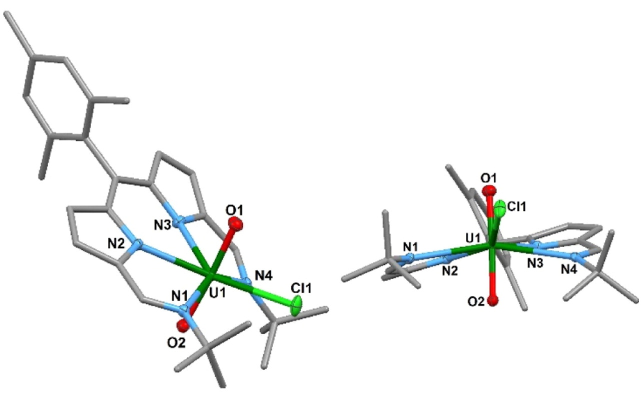

Figure 3. Solid-state structure of $U^{VI}O_2Cl(\mathbf{L}^{\mathbf{Mes}})$ viewed from the top (left) and side (right). For clarity, all hydrogen atoms are omitted (displacement ellipsoids are drawn at 50% probability). Selected bonds distances (Å) and angles (deg): U1−N1, 2.676(2); U1−N2, 2.469(2); U1−N3, 2.477(2); U1−N4, 2.675(2); U1−O1, 1.765(2); U1−O2, 1.768(2); U1−Cl1, 2.6882(7); N1−U1−N2, 65.85(6); N2−U1−N3, 70.30(6); N3−U1−N4, 65.30(6); N4−U1−N1, 152.03(6); N4−U1−Cl1, 79.22(4); N1−U1−Cl1, 87.84(4); and O1−U1−O2, 176.15(8).

center adopts a distorted pentagonal bipyramidal coordination geometry in which the N_4 donor set of the expanded dipyrrin ligand occupies the equatorial positions along with the chloride ligand; this structure is similar to that of $U^{VI}O_2Cl(\mathbf{L}^{\mathbf{F}})$.[11] The Cl1 atom is situated 1.621 Å above the mean N_4 plane and indicates a steric interaction between this ligand and the nearby *tert*-butyl groups. These *tert*-butyl groups bend away from the same face of the N_4 donor plane, meaning that the C_{2v} symmetry observed in the solution state is not retained in the solid state; this feature was also seen in $U^{VI}O_2Cl(\mathbf{L}^{\mathbf{F}})$.[11] The uranium oxo bond distances O1−U1 and U1−O2 are 1.765(2) and 1.768(2) Å, respectively, with an O1−U1−O2 angle of 176.15(8)°. This complex exhibits U═O bond lengths and O═U═O angles in the range of other non-functionalized uranyl(VI) complexes reported since 2010,[2] in which the average U═O bond length is 1.777 Å. The U1−$N_{pyrrole}$ bond lengths are 2.469(2) and 2.477(2) Å, while the U1−N_{imine} bond lengths are 2.676(2) and 2.675(2) Å. The U1−Cl1 bond length is 2.6882(7) Å and similar to that seen in $U^{VI}O_2Cl$-($\mathbf{L}^{\mathbf{F}}$).[11]

Electronic Spectroscopy. The absorbance spectra of $H\mathbf{L}^{\mathbf{Mes}}$, K($\mathbf{L}^{\mathbf{Mes}}$), and $U^{VI}O_2Cl(\mathbf{L}^{\mathbf{Mes}})$ were recorded in anhydrous THF (Figure 4). $H\mathbf{L}^{\mathbf{Mes}}$ has a maximum absorbance

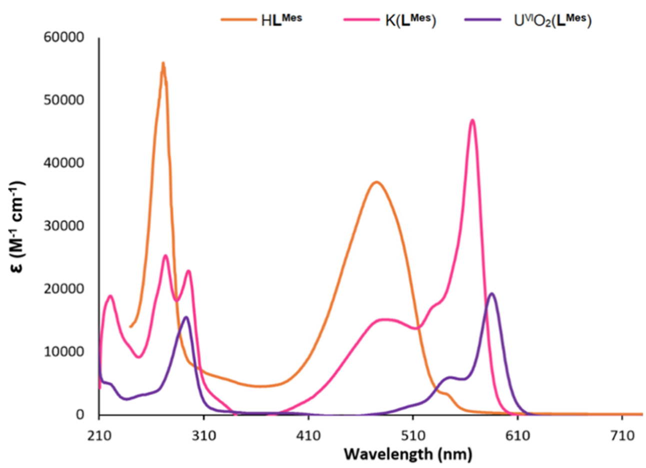

Figure 4. UV−vis spectra of $H\mathbf{L}^{\mathbf{Mes}}$, K($\mathbf{L}^{\mathbf{Mes}}$), and $U^{VI}O_2Cl(\mathbf{L}^{\mathbf{Mes}})$ in anhydrous THF.

of 272 nm (ε = 55 206 M^{-1} cm^{-1}) and a second peak at 476 nm (ε = 36 961 M^{-1} cm^{-1}), which are similar to that for $H\mathbf{L}^{\mathbf{F}}$. Although no time-dependent density functional theory (TD-DFT) calculations have been conducted, the latter absorption band is likely attributed to the ligand-centered $\pi \rightarrow \pi^*$ transition localized on the dipyrrin−diimine fragment. Upon metalation to form the potassium salt K($\mathbf{L}^{\mathbf{Mes}}$), the easy to visualize color change is reflected in the UV−vis spectrum with significant red shifts observed relative to that of $H\mathbf{L}^{\mathbf{Mes}}$ with a maximum absorbance at 568 nm (ε = 46 315 M^{-1} cm^{-1}). The uranyl complex $U^{VI}O_2Cl(\mathbf{L}^{\mathbf{Mes}})$ is red-shifted further and with a decrease in the extinction coefficient, exhibiting a maximum absorbance at 584 nm (ε = 19 210 M^{-1} cm^{-1}) with a shoulder at 539 nm (ε = 5526 M^{-1} cm^{-1}).

Synthesis and Structure of the Uranyl(V) Dimer. The reaction between $U^{VI}O_2Cl(\mathbf{L}^{\mathbf{Mes}})$ and 1 equiv of $CoCp_2$ in benzene results in the precipitation of a golden pink paramagnetic species, which is soluble in pyridine (Scheme 3). The ^1H NMR spectrum in pyridine-d_5 exhibits resonances between +4 and −10 ppm, consistent with the reduction of uranyl(VI) to uranyl(V) and not the formation of a ligand radical. The spectrum depicts five individual mesityl peaks as a result of top/bottom asymmetry. The mesityl CH peaks shift to 3.14 and 1.96 ppm, and the methyl peaks shift to −0.33, −0.59, and −1.90 ppm. The β-pyrrole protons are seen at −4.94 and −5.41 ppm, and the imine proton is observed at

https://doi.org/10.1021/acs.inorgchem.2c03048
Inorg. Chem. 2022, 61, 20424−20432

−9.17 ppm. The *tert*-butyl protons are seen as two singlets at −6.12 and −6.21 ppm, having an area of 2:1, and is consistent with C_2 symmetry.

Goldish-purple plate-shaped crystals were grown by slowly cooling a hot benzene solution, and the solid-state structure of $[U^{V}O_2(\mathbf{L}^{\mathbf{Mes}})]_2$ was determined by X-ray crystallography. The solid-state structure reveals the formation of a uranyl(V) dimer complex $[U^{V}O_2(\mathbf{L}^{\mathbf{Mes}})]_2$ and neither the formation of $[Cp_2Co][U^{V}O_2Cl(\mathbf{L}^{\mathbf{Mes}})]$ nor that of $[Cp_2Co][U^{VI}O_2Cl(\mathbf{L}^{\mathbf{Mes•}})]$ (Figure 5). The solid-state structure shows a

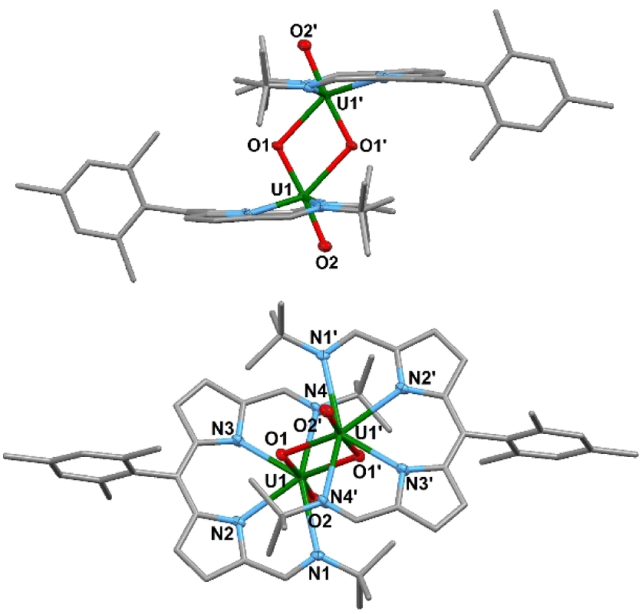

Figure 5. Solid-state structure of $[U^{V}O_2(\mathbf{L}^{\mathbf{Mes}})]_2$ viewed from the side (top) and top (bottom). For clarity, one molecule, one benzene solvate molecule, and all hydrogen atoms are omitted (displacement ellipsoids are drawn at 50% probability). Carbon atoms are gray. Selected bond distances (Å) and angles (deg): U1−U1′, 3.5299(4); U1−N1, 2.694(3); U1−N2, 2.495(3); U1−N3, 2.502(3); U1−N4, 2.665(4); U1−O1, 1.933(3); U1−O2, 1.833(3); U1−O1′, 2.395(3); N1−U1−N2, 65.4(1); N2−U1−N3, 70.6(1); N3−U1−N4, 65.2(1); N4−U1−N1, 150.6(1); O1−U1−O2, 175.5(1); O1−U1−O1′, 70.7(1); O1′−U1−O2, 113.3(1); U1−O1′−U1′, 109.3(1); and U1−O1−U1′, 109.3(1).

diamond-shaped, dioxo-bridge between the two uranium(V) centers. The axial O1−U1 and O2−U1 bond lengths are 1.933(3) and 1.833(3) Å, respectively, and the equatorial O1′−U1 is longer at 2.395(3) Å. The O1−U1−O2 has a bond angle of 175.52°, O2−U1−O1′ has an angle of 113.31°, and O1′−U1−O1 has an angle of 70.74° with a U1⋯U1′ separation of 3.5389(4) Å. The U−O bond lengths of uranyl(V) dioxo complexes reported since 2010 range from 1.77(1) to 2.170(8) Å.[2]

A similar diamond-shaped, dioxo-bridged dimer has been synthesized before from $U^{VI}O_2Cl(\mathbf{L}^{\mathbf{F}})$ through its reaction with 1 equiv of KNHDIPP (Dipp = 2,6-$^{i}Pr_2C_6H_3$).[12] This reduction reaction presumably proceeded through the formation of the transient anilide complex $U^{VI}O_2(NHDipp)(\mathbf{L}^{\mathbf{F}})$, which then underwent U−N bond homolysis.[12,21] The solid-state structure of $[U^{V}O_2(\mathbf{L}^{\mathbf{F}})]_2$ has similar metrics to $[U^{V}O_2(\mathbf{L}^{\mathbf{Mes}})]_2$.[12] The above-described dimers, or the coordination of an actinyl "yl" oxygen to the metal center of another actinyl fragments, are examples of cation−cation interactions, or CCIs, seen in actinide oxo complexes.[22]

Electrochemistry. The cyclic voltammograms (CVs) of $\mathbf{HL}^{\mathbf{Mes}}$, $K(\mathbf{L}^{\mathbf{Mes}})$ and $U^{VI}O_2Cl(\mathbf{L}^{\mathbf{Mes}})$ were recorded in anhydrous CH_2Cl_2 at a scan rate of 100 mV s^{-1} (Figure 6).

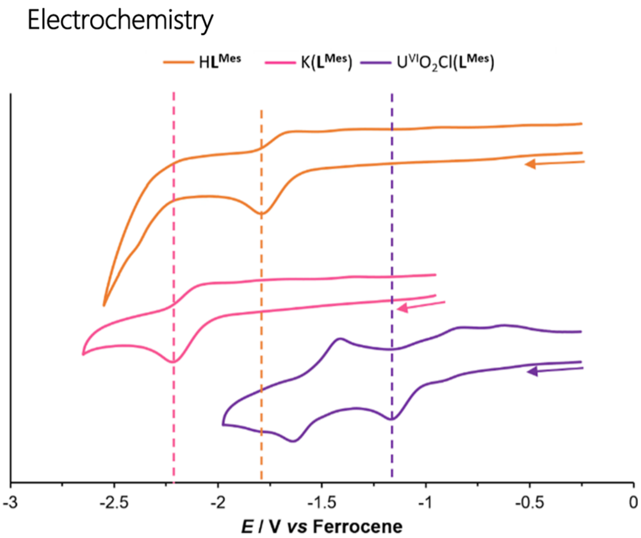

Figure 6. Stacked CVs of $\mathbf{HL}^{\mathbf{Mes}}$, $K(\mathbf{L}^{\mathbf{Mes}})$, and $U^{VI}O_2Cl(\mathbf{L}^{\mathbf{Mes}})$. All were measured as 1 mM anhydrous CH_2Cl_2 solutions (a 1.0 M $[^{n}Bu_4N][PF_6]$ supporting electrolyte, a glassy carbon working electrode, a Pt gauze counter electrode, and a silver wire quasi-reference electrode). Potentials are referenced against Fc/Fc^+ couple recorded under identical conditions.

The CV of $\mathbf{HL}^{\mathbf{Mes}}$ features a quasi-reversible reduction at $E_{1/2}$ −1.72 V *versus* Fc/Fc^+ and an irreversible reduction at E_{pc} −2.40 V *versus* Fc/Fc^+. In comparison, $\mathbf{HL}^{\mathbf{F}}$ displayed a significantly less-negative reduction of E_{pc} −1.51 V *versus* Fc/Fc^+, showing that the electron-withdrawing *meso*-carbon substituent facilitates ligand reduction.[11] The CV of $K(\mathbf{L}^{\mathbf{Mes}})$ features a single quasi-reversible reduction at $E_{1/2}$ −2.15 V *versus* Fc/Fc^+.

The first reduction peaks of $\mathbf{HL}^{\mathbf{Mes}}$ and $K(\mathbf{L}^{\mathbf{Mes}})$ are quasi-reversible, and it can therefore be concluded that the radical species $[\mathbf{HL}^{\mathbf{Mes•}}]^-$ and $[K(\mathbf{L}^{\mathbf{Mes•}})]^-$ are unstable under the cyclic voltammetry conditions. These features are more reversible with an increased scan rate (see the Supporting Information).

The CV of $U^{VI}O_2Cl(\mathbf{L}^{\mathbf{Mes}})$ features two different redox processes upon cathodic scanning, the first being an irreversible wave at −1.15 V *versus* Fc/Fc^+ and the second being a quasi-reversible reduction wave at −1.54 V *versus* Fc/Fc^+. This is different from the CV of $U^{VI}O_2Cl(\mathbf{L}^{\mathbf{F}})$ since this compound features three quasi-reversible reduction processes at $E_{1/2}$ of−0.96, −1.18, and −2.02 V *versus* Fc/Fc^+, corresponding with the ligand reduction, $U^{VI/V}$, and $U^{V/IV}$ reduction, respectively (Table 1). The CV of $U^{VI}O_2Cl(\mathbf{L}^{\mathbf{Mes}})$ does, however, bear resemblance to that of the cationic compound $[U^{VI}O_2(\mathbf{L}^{\mathbf{F}})][BAr^F]$ (BAr^F = tetrakis[3,5-bis-(trifluoromethyl)phenyl]borate),[12] which showed an irreversible reduction at −0.64 V *versus* Fc/Fc^+ and a quasi-reversible reduction wave at −1.24 V. The first reduction of $[U^{VI}O_2(\mathbf{L}^{\mathbf{F}})][BAr^F]$ was assigned as the U^{VI}/U^{V} couple with its irreversibility indicating the formation of the U^{V} dimer

https://doi.org/10.1021/acs.inorgchem.2c03048
Inorg. Chem. 2022, 61, 20424−20432

Table 1. Cyclic Voltammetry Data

complex	process	E_{pc} (V)	E_{pa} (V)	ΔE (V)	$E_{1/2}$ (V)	reversibility	red/ox	assignment
HL^{Mes}	I	−1.80	−1.66	0.14	−1.72	quasi-reversible	reduction	$L^-/L^{•-}$
	II	−2.40				irreversible	reduction	$L^{•-}/L^{3-}$
HL^{F}[11]	I	−1.51				Irreversible	reduction	$L^-/L^{•-}$
	II	−2.02				irreversible	reduction	$L^{•-}/L^{3-}$
$K(L^{Mes})$	I				−2.15	quasi-reversible	reduction	$L^-/L^{•-}$
$K(L^{F})$[11]	I	−1.29				irreversible	reduction	$L^-/L^{•-}$
	II	−1.57				irreversible	reduction	$L^{•-}/L^{3-}$
$U^{VI}O_2Cl(L^{Mes})$	I	−1.15				irreversible	reduction	$L^-/L^{•-}$
	II	−1.64	−1.43	0.21	−1.54	quasi-reversible	reduction	U^{VI}/U^{V}
$U^{VI}O_2Cl(L^{F})$[11]	I	−1.03	−0.89	0.14	−0.96	quasi-reversible	reduction	$L^-/L^{•-}$
	II	−1.25	−1.10	0.15	−1.18	quasi-reversible	reduction	U^{VI}/U^{V}
	III	−2.10	−1.94	0.16	−2.02	quasi-reversible	reduction	U^{V}/U^{IV}
$[U^{VI}O_2(L^{F})][BarF]$[12]	I	−0.64				irreversible	reduction	U^{VI}/U^{V}
	II	−1.37	−1.12	0.25	−1.24	quasi-reversible	reduction	U^{V}/U^{IV}

$[U^VO_2(L^F)]_2$; the second peak was assigned as reduction to U^{IV}.[12]

Electron Paramagnetic Resonance Spectroscopy. Although the CVs depicted similarities between $U^{VI}O_2Cl(L^{Mes})$ and $[U^{VI}O_2(L^F)][BAr^F]$, electron paramagnetic resonance (EPR) analysis was still carried out on the reduction of $U^{VI}O_2Cl(L^{Mes})$ to rule out ligand reduction. As such, $U^{VI}O_2Cl(L^{Mes})$ was reacted with $CoCp_2$ in anhydrous CH_2Cl_2 at ambient temperature and monitored. The EPR shows the formation of $[U^{VI}O_2Cl(L^{Mes•})]^-$ with a g_{iso} value of 1.987 (Figure 7). There is unresolved hyperfine coupling that gives rise to this unique line shape that is the consequence of perturbed molecular tumbling in solution and line broadening driven by spin−orbital contribution from U^{VI}. The g_{iso} value of $[Cp_2Co][U^{VI}O_2Cl(L^{F•})]$ was similar at 1.9893, and the shape of the signal is consistent with the carbon radical.[11] The observation of this EPR signal suggests that the formation of the isolated dimer uranyl(V) complex proceeds *via* the one-electron reduction of the ligand and thus through the formation of a ligand radical complex $[U^{VI}O_2Cl(L^{Mes•})]^-$.

The *g*-value is slightly lower in comparison to that of the free electron, which is due to the interaction of the unpaired spin with the larger spin−orbital coupling associated with the uranium nucleus. Other reported $U^{VI}-(L^•)$ species display similar *g*-values and line broadening in their fluid solution EPR spectra.[11,23] In each case, the unpaired spin was assigned to the ligand moiety, with the low *g*-values due to spin−orbital coupling to the uranium center.[3]

DFT Calculations. A variety of DFT calculations were undertaken on both $U^{VI}O_2Cl(L^{Mes})$ and $U^{VI}O_2Cl(L^F)$ and reveal that for both the cases, the LUMOs are located entirely on the ligand, indicating that the incorporation of the electron-donating *meso*-mesityl substituent does not modify the molecular orbitals to a great extent (Figure 8). In addition, the singly occupied molecular orbitals of $[U^{VI}O_2Cl(L^{Mes•})]^-$ and $[U^{VI}O_2Cl(L^{F•})]^-$ are also ligand-based, and the unpaired spin density maps of both show that the electron density is located on the ligand, primarily on the *meso*-carbon, and not on the uranium atom; this further confirms the radical character of the ligand after one-electron reduction.

This reduction process is supported by the solid-state structure obtained for $[Cp_2Co][U^{VI}O_2Cl(L^{F•})]$.[11] However, it is clear that from the experimental reduction of the *meso*-mesityl complex $U^{VI}O_2Cl(L^{Mes})$, only the uranyl(V) dimer

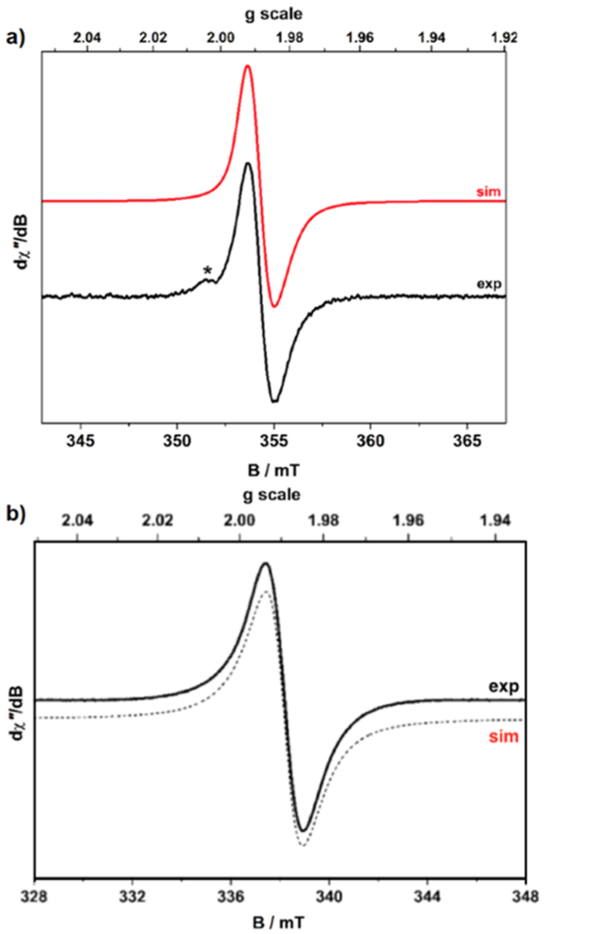

Figure 7. X-Band EPR spectra of $[U^{VI}O_2Cl(L^{Mes•})]^-$ (a) and $[U^{VI}O_2Cl(L^{F•})]^-$ (b) generated in anhydrous CH_2Cl_2 solution at ambient temperature. The measured spectra are shown in black solid lines, and the simulated spectra are shown in dashed black and solid red lines.

$[U^VO_2(L^{Mes})]_2$ is obtained, which is not rationalized through this ligand reduction process.

The similarity in the CVs of $U^{VI}O_2Cl(L^{Mes})$ and the cationic uranyl complex $[U^{VI}O_2(L^F)][BAr^F]$ suggests that reduction is in concert with chloride dissociation (Scheme 4). This step was computed and results in the formation of $U^{VI}O_2(L^{Mes•})$ and $U^{VI}O_2(L^{F•})$, which are energetically plausible for both

https://doi.org/10.1021/acs.inorgchem.2c03048
Inorg. Chem. 2022, 61, 20424−20432

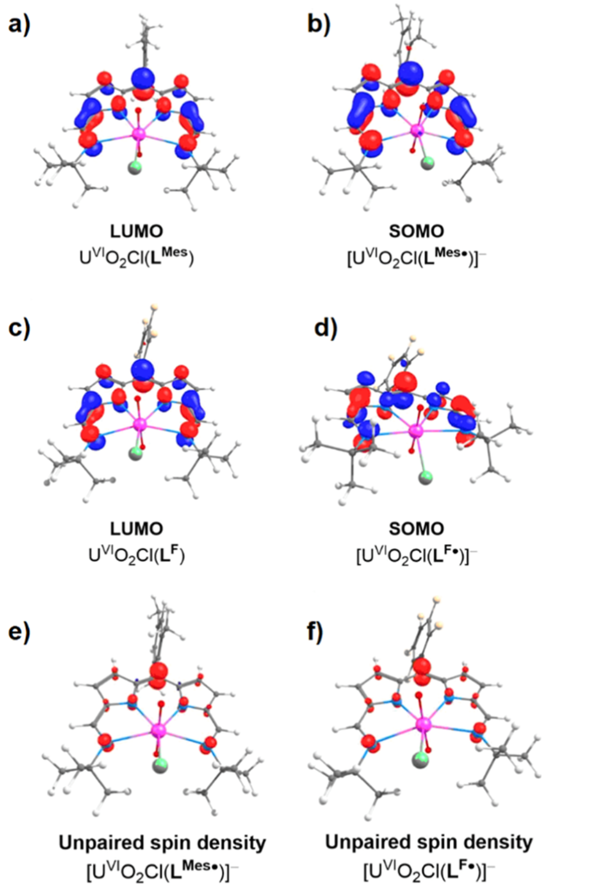

Figure 8. Molecular orbital plots of $U^{VI}O_2Cl(\mathbf{L^{Mes}})$ and $[U^{VI}O_2Cl(\mathbf{L^{Mes\bullet}})]^-$ (a,b) and $U^{VI}O_2Cl(\mathbf{L^F})$ and $[U^{VI}O_2Cl(\mathbf{L^{F\bullet}})]^-$ (c,d) and spin density plots of the singly reduced complexes $[U^{VI}O_2Cl(\mathbf{L^\bullet})]^-$ (e,f). The ISO value is 0.02 au. Positive is blue; negative is red.

complexes at +20 kcal mol^{-1} for $U^{VI}O_2(\mathbf{L^{Mes\bullet}})$ and +21 kcal mol^{-1} for $U^{VI}O_2(\mathbf{L^{F\bullet}})$. In both cases, electron transfer from the ligand to the metal does not occur.

The next computed step involves the formation of a U^V–(**L**) monomer through electron transfer from the ligand to the metal, thus forming $U^VO_2(\mathbf{L^{Mes}})$ and $U^VO_2(\mathbf{L^F})$, respectively. This step is estimated to cost +15 kcal mol^{-1} for the $U^VO_2(\mathbf{L^{Mes}})$ and +26 kcal mol^{-1} for $U^VO_2(\mathbf{L^F})$. Therefore, the former formation is thermally accessible at +35 kcal mol^{-1} from $U^{VI}O_2Cl(\mathbf{L^{Mes}})$ but inaccessible for $U^VO_2(\mathbf{L^F})$ at +47 kcal mol^{-1}. It is important to note that dimerization of the monomeric uranyl(V) complex $U^VO_2(\mathbf{L^{Mes}})$ to form the uranyl(V) dimer $[U^VO_2(\mathbf{L^{Mes}})]_2$ is exothermic by −45 kcal mol^{-1}, making the whole process exothermic by 10 kcal mol^{-1}.

■ DISCUSSION

Changing the meso substituent of the dipyrrin ligand in the uranyl complexes $U^{VI}O_2Cl(\mathbf{L})$ from electron-withdrawing $\mathbf{L^F}$ to electron-donating $\mathbf{L^{Mes}}$ modifies the stability of the products formed upon single-electron reduction; for $\mathbf{L^F}$, the ligand-reduced complex $U^{VI}O_2Cl(\mathbf{L^{F\bullet}})$ is isolated, whereas in contrast, for $\mathbf{L^{Mes}}$, the uranyl(V) dimer $[U^VO_2(\mathbf{L^{Mes}})]_2$ is seen. This difference in the reduction product is also implied experimentally from the differences in the CVs of these complexes and the instability of the singly reduced complex $[U^{VI}O_2Cl(\mathbf{L^{Mes\bullet}})]^-$ by EPR spectroscopy.

Scheme 4. Reduction Processes for $U^{VI}O_2Cl(L^{Mes})$ and $U^{VI}O_2Cl(L^F)$ Resulting in $[U^VO_2(L^{Mes})]_2$ and $[Cp_2Co][U^{VI}O_2CL(L^{F\bullet})]$, Respectively

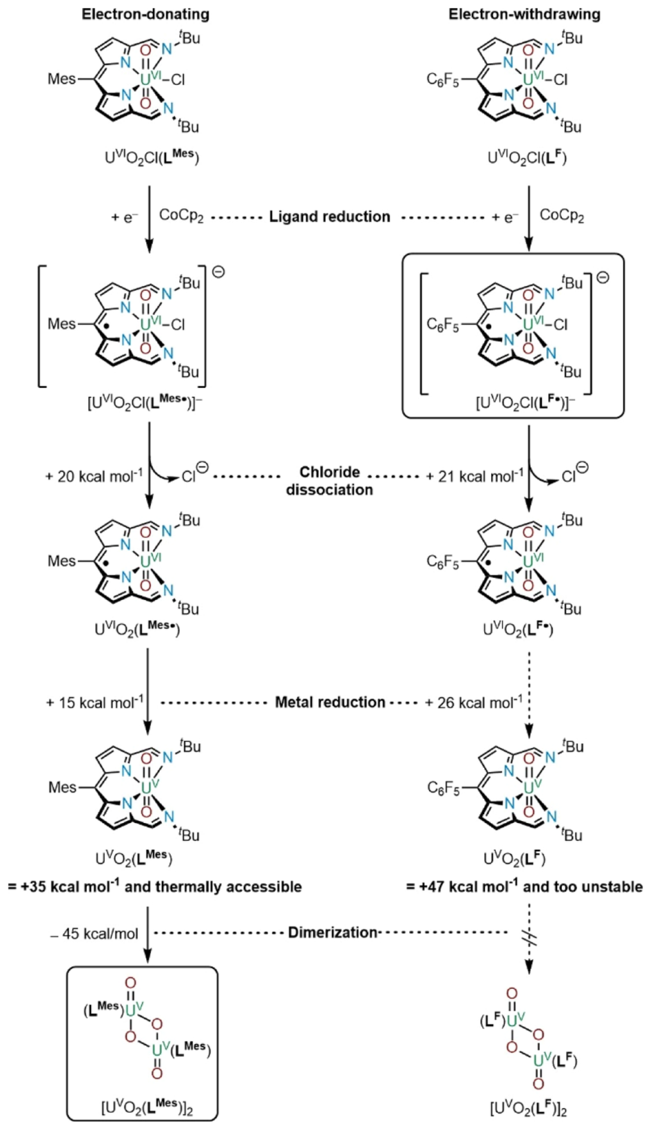

The difference in reactivity caused by the mesityl meso substituent becomes clear when analyzing the different steps of the reduction processes computationally. Although both $U^{VI}O_2Cl(\mathbf{L^{Mes}})$ and $U^{VI}O_2Cl(\mathbf{L^F})$ can form the chloride-free ligand–radical complexes $U^{VI}O_2(\mathbf{L^{Mes\bullet}})$ and $U^{VI}O_2(\mathbf{L^{F\bullet}})$, respectively, only the mesityl analogue undergoes an electron transfer from the ligand to the metal. The latter process requires an increase in energy of 11 kcal mol^{-1} for the pentafluorophenyl analogue, making it thermally inaccessible. It is therefore shown that the pentafluorophenyl substituent stabilizes the ligand–radical complex, causing electron transfer to the metal to be less favorable, whereas the mesityl substituent destabilizes the ligand–radical complexes, facilitating the electron transfer. Once the $U^VO_2(\mathbf{L^{Mes}})$ monomer is formed, the formation of the diamond-shaped, oxo-bridged uranyl(V) dimer is facile and is promoted by the increased Lewis basicity of the axial oxos of the reduced uranyl center.[24]

https://doi.org/10.1021/acs.inorgchem.2c03048
Inorg. Chem. 2022, 61, 20424−20432

■ CONCLUSIONS

We have shown that the variation of the meso substituent in uranyl Schiff-base dipyrrin complexes moderates the stabilities of the neutral, ligand-reduced complexes $U^{VI}O_2(\mathbf{L}^{\bullet})$, which affects the subsequent electron transfer to the metal. It is anticipated that further modification of the dipyrrin ligand, for example, increasing the steric bulk at the α-positions of the pyrrole or substituting at the β-positions, could lead to the formation of new uranyl(V) products by suppressing dimerization. Furthermore, the facile ligand modifications described here may prove important in the design of future reactions such as electron transfer or oxo-atom transfer in which controlled access to either the ligand radical or uranyl(V) complexes is desired.

■ ASSOCIATED CONTENT

Supporting Information

The Supporting Information is available free of charge at https://pubs.acs.org/doi/10.1021/acs.inorgchem.2c03048.

Additional synthetic procedures, X-ray crystallography, DFT calculations, EPR spectroscopy, and electrochemical methods (PDF)

Accession Codes

CCDC 2201750–2201753 contain the supplementary crystallographic data for this paper. These data can be obtained free of charge via www.ccdc.cam.ac.uk/data_request/cif, or by emailing data_request@ccdc.cam.ac.uk, or by contacting The Cambridge Crystallographic Data Centre, 12 Union Road, Cambridge CB2 1EZ, UK; fax: +44 1223 336033.

■ AUTHOR INFORMATION

Corresponding Author

Jason B. Love – *EaStCHEM School of Chemistry, The University of Edinburgh, Edinburgh EH9 3FJ, U.K.*; orcid.org/0000-0002-2956-258X; Email: Jason.Love@ed.ac.uk

Authors

Karlotta van Rees – *EaStCHEM School of Chemistry, The University of Edinburgh, Edinburgh EH9 3FJ, U.K.*

Thayalan Rajeshkumar – *LPCNO, INSA, Université de Toulouse, Toulouse Cedex 4 31077, France*

Laurent Maron – *LPCNO, INSA, Université de Toulouse, Toulouse Cedex 4 31077, France*; orcid.org/0000-0003-2653-8557

Stephen Sproules – *WestCHEM School of Chemistry, University of Glasgow, Glasgow G12 8QQ, U.K.*; orcid.org/0000-0003-3587-0375

Complete contact information is available at: https://pubs.acs.org/10.1021/acs.inorgchem.2c03048

Author Contributions

This manuscript was written through contributions of all authors. All authors have given approval to the final version of the manuscript.

Notes

The authors declare no competing financial interest.

■ ACKNOWLEDGMENTS

The authors thank the University of Edinburgh, the EPSRC (UK), and the EPSRC CRITICAT Centre for Doctoral Training (PhD studentship to K.v.R.; grant EP/L016419/1) for financial support and the Mass Spectrometry Facility at the University of Edinburgh for carrying out air-sensitive high-resolution mass sepctroscopy analysis.

■ REFERENCES

(1) Cumberland, S. A.; Douglas, G.; Grice, K.; Moreau, J. W. Uranium mobility in organic matter-rich sediments: A review of geological and geochemical processes. *Earth-Sci. Rev.* **2016**, *159*, 160–185.

(2) Cowie, B. E.; Purkis, J. M.; Austin, J.; Love, J. B.; Arnold, P. L. Thermal and Photochemical Reduction and Functionalization Chemistry of the Uranyl Dication, $[U^{VI}O_2]^{2+}$. *Chem. Rev.* **2019**, *119*, 10595–10637.

(3) Herasymchuk, K.; Chiang, L.; Hayes, C. E.; Brown, M. L.; Ovens, J. S.; Patrick, B. O.; Leznoff, D. B.; Storr, T. Synthesis and electronic structure determination of uranium(VI) ligand radical complexes. *Dalton Trans.* **2016**, *45*, 12576–12586.

(4) Bejger, C.; Tian, Y.-H.; Barker, B. J.; Boland, K. S.; Scott, B. L.; Batista, E. R.; Kozimor, S. A.; Sessler, J. L. Synthesis and characterization of a tetrathiafulvalene-salphen actinide complex. *Dalton Trans.* **2013**, *42*, 6716–6719.

(5) (a) Horeglad, P.; Nocton, G.; Filinchuk, Y.; Pécaut, J.; Mazzanti, M. Pentavalent uranyl stabilized by a dianionic bulky tetradentate ligand. *Chem. Commun.* **2009**, 1843–1845. (b) Nocton, G.; Horeglad, P.; Vetere, V.; Pécaut, J.; Dubois, L.; Maldivi, P.; Edelstein, N. M.; Mazzanti, M. Synthesis, Structure, and Bonding of Stable Complexes of Pentavalent Uranyl. *J. Am. Chem. Soc.* **2010**, *132*, 495–508. (c) Mougel, V.; Pécaut, J.; Mazzanti, M. New polynuclear U(IV)–U(V) complexes from U(IV) mediated uranyl(V) disproportionation. *Chem. Commun.* **2012**, *48*, 868–870.

(6) Coughlin, E. J.; Qiao, Y.; Lapsheva, E.; Zeller, M.; Schelter, E. J.; Bart, S. C. Uranyl Functionalization Mediated by Redox-Active Ligands: Generation of O–C Bonds via Acylation. *J. Am. Chem. Soc.* **2019**, *141*, 1016–1026.

(7) Assefa, M. K.; Pedrick, E. A.; Wakefield, M. E.; Wu, G.; Hayton, T. W. Oxidation of the 14-Membered Macrocycle Dibenzotetramethyltetraaza[14]annulene upon Ligation to the Uranyl Ion. *Inorg. Chem.* **2018**, *57*, 8317–8324.

(8) (a) Hayton, T. W.; Wu, G. Synthesis, Characterization, and Reactivity of a Uranyl β-Diketiminate Complex. *J. Am. Chem. Soc.* **2008**, *130*, 2005–2014. (b) Schettini, M. F.; Wu, G.; Hayton, T. W. Coordination of N-Donor Ligands to a Uranyl(V) β-Diketiminate Complex. *Inorg. Chem.* **2009**, *48*, 11799–11808.

(9) Kent, G. T.; Murillo, J.; Wu, G.; Fortier, S.; Hayton, T. W. Coordination of Uranyl to the Redox-Active Calix[4]pyrrole Ligand. *Inorg. Chem.* **2020**, *59*, 8629–8634.

(10) (a) Bolotaulo, D.; Metta-Magaña, A.; Fortier, S. F-element metalated dipyrrins: synthesis and characterization of a family of uranyl bis(dipyrrinate) complexes. *Dalton Trans.* **2017**, *46*, 3284–3294. (b) van Rees, K.; Hield, E. K.; Carpentier, A.; Maron, L.; Sproules, S.; Love, J. B. Exploring the Redox Properties of Bench-Stable Uranyl(VI) Diamido–Dipyrrin Complexes. *Inorg. Chem.* **2022**, *61*, 3249–3255.

(11) Pankhurst, J. R.; Bell, N. L.; Zegke, M.; Platts, L. N.; Lamfsus, C. A.; Maron, L.; Natrajan, L. S.; Sproules, S.; Arnold, P. L.; Love, J. B. Inner-sphere vs. outer-sphere reduction of uranyl supported by a redox-active, donor-expanded dipyrrin. *Chem. Sci.* **2017**, *8*, 108–116.

(12) Bell, N. L.; Shaw, B.; Arnold, P. L.; Love, J. B. Uranyl to Uranium(IV) Conversion through Manipulation of Axial and Equatorial Ligands. *J. Am. Chem. Soc.* **2018**, *140*, 3378–3384.

(13) (a) Takeyama, T.; Tsushima, S.; Takao, K. Effects of Substituents on the Molecular Structure and Redox Behavior of Uranyl(V/VI) Complexes with N_3O_2-Donating Schiff Base Ligands. *Inorg. Chem.* **2021**, *60*, 11435–11449. (b) Takao, K.; Kato, M.; Takao, S.; Nagasawa, A.; Bernhard, G.; Hennig, C.; Ikeda, Y. Molecular Structure and Electrochemical Behavior of Uranyl(VI) Complex with Pentadentate Schiff Base Ligand: Prevention of

Uranyl(V) Cation−Cation Interaction by Fully Chelating Equatorial Coordination Sites. *Inorg. Chem.* **2010**, *49*, 2349−2359.

(14) Takao, K.; Tsushima, S.; Ogura, T.; Tsubomura, T.; Ikeda, Y. Experimental and Theoretical Approaches to Redox Innocence of Ligands in Uranyl Complexes: What Is Formal Oxidation State of Uranium in Reductant of Uranyl(VI)? *Inorg. Chem.* **2014**, *53*, 5772−5780.

(15) (a) Faizova, R.; Fadaei-Tirani, F.; Chauvin, A.-S.; Mazzanti, M. Synthesis and Characterization of Water Stable Uranyl(V) Complexes. *Angew. Chem., Int. Ed.* **2021**, *60*, 8227−8235. (b) Faizova, R.; Scopelliti, R.; Chauvin, A.-S.; Mazzanti, M. Synthesis and Characterization of a Water Stable Uranyl(V) Complex. *J. Am. Chem. Soc.* **2018**, *140*, 13554−13557.

(16) (a) Shikha Singh, R.; Prasad Paitandi, R.; Kumar Gupta, R.; Shankar Pandey, D. Recent developments in metal dipyrrin complexes: Design, synthesis, and applications. *Coord. Chem. Rev.* **2020**, *414*, 213269. (b) Baudron, S. A. Dipyrrin based metal complexes: reactivity and catalysis. *Dalton Trans.* **2020**, *49*, 6161−6175.

(17) (a) Sheldrick, G. M. SHELXT-Integrated Space-Group and Crystal-Structure Determination. *Acta Crystallogr., Sect. A: Found. Adv.* **2015**, *71*, 3−8. (b) Sheldrick, G. M. Crystal Structure Refinement with SHELXL. *Acta Crystallogr., Sect. C: Struct. Chem.* **2015**, *71*, 3−8. (c) Sheldrick, G. M. A short history of SHELX. *Acta Crystallogr., Sect. A: Found. Adv.* **2008**, *64*, 112.

(18) Dolomanov, O. V.; Bourhis, L. J.; Gildea, R. J.; Howard, J. A. K.; Puschmann, H. OLEX2: a complete structure solution, refinement and analysis program. *J. Appl. Crystallogr.* **2009**, *42*, 339−341.

(19) (a) Sessler, J. L.; Seidel, D.; Bucher, C.; Lynch, V. Novel, terpyrrole-containing, aromatic expanded porphyrins. *Tetrahedron* **2001**, *57*, 3743−3752. (b) Littler, B. J.; Miller, M. A.; Hung, C.-H.; Wagner, R. W.; O'Shea, D. F.; Boyle, P. D.; Lindsey, J. S. Refined Synthesis of 5-Substituted Dipyrromethanes. *J. Org. Chem.* **1999**, *64*, 1391−1396.

(20) (a) van Rees, K.; Love, J. Synthesis and complexes of a constrained-cavity Schiff-base dipyrrin macrocycle. *Dalton Trans.* **2021**, *50*, 1610−1613. (b) Pankhurst, J. R.; Cadenbach, T.; Betz, D.; Finn, C.; Love, J. B. Towards dipyrrins: oxidation and metalation of acyclic and macrocyclic Schiff-base dipyrromethanes. *Dalton Trans.* **2015**, *44*, 2066−2070.

(21) Berthet, J.-C.; Siffredi, G.; Thuéry, P.; Ephritikhine, M. Synthesis and crystal structure of pentavalent uranyl complexes. The remarkable stability of UO_2X (X = I, SO_3CF_3) in non-aqueous solutions. *Dalton Trans.* **2009**, *18*, 3478−3494.

(22) (a) Arnold, P. L.; Hollis, E.; Nichol, G. S.; Love, J. B.; Griveau, J.-C.; Caciuffo, R.; Magnani, N.; Maron, L.; Castro, L.; Yahia, A.; Odoh, S. O.; Schreckenbach, G. Oxo-Functionalization and Reduction of the Uranyl Ion through Lanthanide-Element Bond Homolysis: Synthetic, Structural, and Bonding Analysis of a Series of Singly Reduced Uranyl−Rare Earth 5f1-4fn Complexes. *J. Am. Chem. Soc.* **2013**, *135*, 3841−3854. (b) Cornet, S. M.; Häller, L. J. L.; Sarsfield, M. J.; Collison, D.; Helliwell, M.; May, I.; Kaltsoyannis, N. Neptunium(VI) chain and neptunium(VI/V) mixed valence cluster complexes. *Chem. Commun.* **2009**, *8*, 917−919. (c) Fortier, S.; Hayton, T. W. Oxo ligand functionalization in the uranyl ion (UO_2^{2+}). *Coord. Chem. Rev.* **2010**, *254*, 197−214. (d) Burdet, F.; Pécaut, J.; Mazzanti, M. Isolation of a Tetrameric Cation−Cation Complex of Pentavalent Uranyl. *J. Am. Chem. Soc.* **2006**, *128*, 16512−16513. (e) Krot, N. N.; Grigoriev, M. S. Cation—cation interaction in crystalline actinide compounds. *Russ. Chem. Rev.* **2004**, *73*, 89−100.

(23) (a) Melfi, P. J.; Kim, S. K.; Lee, J. T.; Bolze, F.; Seidel, D.; Lynch, V. M.; Veauthier, J. M.; Gaunt, A. J.; Neu, M. P.; Ou, Z.; Kadish, K. M.; Fukuzumi, S.; Ohkubo, K.; Sessler, J. L. Redox Behavior of Cyclo[6]pyrrole in the Formation of a Uranyl Complex. *Inorg. Chem.* **2007**, *46*, 5143−5145. (b) Anderson, N. H.; Odoh, S. O.; Williams, U. J.; Lewis, A. J.; Wagner, G. L.; Lezama Pacheco, J.; Kozimor, S. A.; Gagliardi, L.; Schelter, E. J.; Bart, S. C. Investigation of the Electronic Ground States for a Reduced Pyridine(diimine) Uranium Series: Evidence for a Ligand Tetraanion Stabilized by a Uranium Dimer. *J. Am. Chem. Soc.* **2015**, *137*, 4690−4700. (c) Kiernicki, J. J.; Cladis, D. P.; Fanwick, P. E.; Zeller, M.; Bart, S. C. Synthesis, Characterization, and Stoichiometric U−O Bond Scission in Uranyl Species Supported by Pyridine(diimine) Ligand Radicals. *J. Am. Chem. Soc.* **2015**, *137*, 11115−11125.

(24) Arnold, P. L.; Love, J. B.; Patel, D. Pentavalent uranyl complexes. *Coord. Chem. Rev.* **2009**, *253*, 1973−1978.

https://doi.org/10.1021/acs.inorgchem.2c03048
Inorg. Chem. 2022, 61, 20424−20432